ORGANIC CHEMISTRY FRONTIERS

RESEARCH ARTICLE

View Article Online
View Journal

Cite this: DOI: 10.1039/d3qo01021j

Sodiated Oppolzer enolates: solution structures, mechanism of alkylation, and origin of stereoselectivity†

Nathan M. Lui and David B. Collum *

NMR spectroscopic studies reveal camphorsultam-derived sodium enolates known as Oppolzer enolates reside as monomers in neat THF and THF/HMPA solutions and as dimers in toluene when solvated by *N,N,N′,N′*-tetramethylethylenediamine (TMEDA) and *N,N,N′,N″,N″*-pentamethyldiethylenediamine (PMDTA). Density functional theory (DFT) computations attest to the solvation numbers. Rate studies show analogy with previously studied lithiated Oppolzer enolates in which alkylation occurs through non-chelated solvent-separated ion pairs. The origins of the selectivity trace to transition structures in which the alkylating agent is guided to the *exo* face of the camphor owing to stereoelectronic preferences imparted by the sultam sulfonyl moiety. Marked secondary-shell solvation effects are gleaned from the rate studies.

Received 4th July 2023,
Accepted 14th August 2023

DOI: 10.1039/d3qo01021j

rsc.li/frontiers-organic

Introduction

Alkylations of camphorsultam-derived enolates referred to colloquially as Oppolzer enolates have occupied a central position in asymmetric synthesis (eqn (1)).[1] In addition to the relatively low-cost auxiliary, there is an unmistakable appeal to the widely held logic that a chelate of type **1** imparts rigidity while the camphor methyl protruding above the enolate directs the electrophile to the *endo* face of the bicyclo[2.2.1]heptane ring system. The Oppolzer enolates merged our interest in understanding the structure–reactivity-selectivity relationships of alkali metal enolates[2] with efforts to promote the long-overlooked potential of organosodium chemistry.[3]

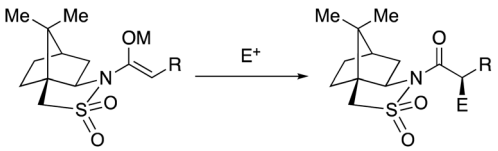

(1)

In the first of a two-part study, we explored the structures of alkyl- and aryl-substituted lithiated Oppolzer enolates in a variety of solvents and their reactivities in THF/HMPA.[4] Focusing on the aryl cases was justified by a notable lack of their development for generating medicinally important aryl propionate derivatives,[5] and they were more tractable in what proved to be a complex study under the best of circumstances. There are, of course, always surprises when one probes alkali metal chemistry, the most poignant in that study was that the alkylation proceeds *via* a mechanism based on a solvent-separated ion pair (**2**). The enolate showed a marked preference to rotate nearly 180 degrees relative to chelate **1** with the preferred facial attack coming from the *exo* face proximate to the protruding camphor methyl. Needless to say, the irrelevance of chelation, the counterion, and even van der Waals interactions with the camphor methyl moiety flew in the face of conventional wisdom. We attributed the high selectivity to a *stereoelectronic* preference of the electrophile to approach *anti* to the *endo*-oriented sulfonyl oxygen.

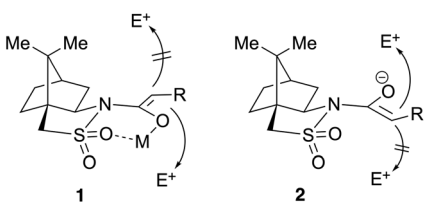

Our motivations to examine the sodium enolates focused on confirming or refuting the stereochemical model in which the alkali metal cation was simply a counterion of little structural importance. We immediately confronted the first challenge: unbeknownst to us and probably the practitioners who routinely use NaHMDS/THF to enolize the acylated Oppolzer sultam,[6,7] the alkyl-substituted substrates (**3a–f** below) are only partially ($K_{eq.}$ < 1) metalated by NaHMDS (eqn (2)).[8] Although the transiently formed sodium enolate appears to be adequate

Department of Chemistry and Chemical Biology, Baker Laboratory, Cornell University, Ithaca, New York 14853-1301, USA. E-mail: dbc6@cornell.edu

†Electronic supplementary information (ESI) available: Synthetic and experimental procedures, spectroscopic, rate, and computational data. See DOI: https://doi.org/10.1039/d3qo01021j

for the applications, the lack of full enolization makes enolate structure–reactivity relationships elusive.

We considered several approaches to overcoming this issue. First, rate studies with NaHMDS and alkyl-substituted sultams as the resting state would provide detailed insights into the mechanism of the enolate alkylation and were appealing given the detailed understanding of the aggregation and solvation of NaHMDS in solution.[3a] Second, we could retreat to the aryl-substituted cases that are quantitatively metalated, which also allows direct comparisons with the aryl-substituted lithium enolates. Third, a stronger base would readily generate the alkyl- and aryl-substituted enolates quantitatively. Although sodium diisopropylamide (NaDA) offers more than adequate basicity,[3b] the excellent stability and solubility profiles of sodium isopropyl(trimethylsilyl) amide (NaPTA) with an additional 4–5 pK_b units above NaHMDS make it a far superior choice (eqn (2)).[3c]

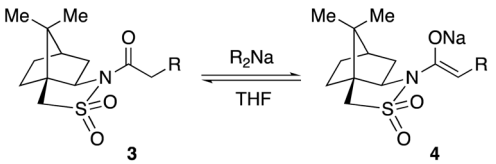

3 4 (2)

NaHMDS: $K_{eq} < 1$

i-Pr(Me_3Si)NNa: $K_{eq} >> 1$

We describe herein studies showing a high penchant for sodiated Oppolzer enolates to reside as monomers in THF solution and dimers when solvated by *N*,*N*,*N*′,*N*′-tetramethylethylenediamine (TMEDA) and *N*,*N*,*N*′,*N*″,*N*″-pentamethylethylene triamine (PMDTA) in toluene. Rate studies show that the ion-pair-based model represented by **2** held firm. The results also shed light on the role of HMPA and how two research groups managed to omit the HMPA through careful control of reaction conditions.[7]

Results and discussion

As foreshadowed in the introduction, the alkyl-substituted substrates **3a–f** (Scheme 1) require the more basic NaPTA.[3c] Substrates **3g–j** bearing aryl substituents were enolized using solutions of NaHMDS or NaPTA in a variety of solvents including toluene, MTBE, and THF. Enolates solvated by diamine TMEDA and triamine PMDTA were generated in toluene. Aging studies revealed no evidence of temperature-dependent aggregate changes and that decomposition commenced above 0 °C.

We routinely determine enolate aggregation states using the Method of Continuous Variations (MCV)[3a,4,9] in which binary mixtures of structurally similar enolates or even enolate enantiomers afford heteroaggregates whose number, symmetries, and mole-fraction dependencies monitored using ^{13}C, ^{1}H, or ^{19}F NMR spectroscopies attest to the aggregation states of the homoaggregates. This study, however, is dominated by monomeric enolates in THF wherein binary mixtures of either aryl- or alkyl-substituted enolates afford no heteroaggregates. Density functional theory (DFT) computations provided best-guess solvation numbers of the monomers,[10–12] which we use to interpret the rate data.

THF

Two enolates showing lack of heteroaggregation are illustrated in Fig. 1. The region of the ^{13}C NMR spectrum shown affords the most well-resolved hetero- and homoaggregate resonances when heteroaggregates appear (*vide infra*). Analogous pairings showing no additional resonances expected for heteroaggregates are in the ESI.† Both aryl- and alkyl-substituted enolates are monomeric in neat THF. The rate studies described are also consistent with the monomer assignment. DFT computations on enolate **4g** suggest di-, tri-, and tetrasolvated *exo*-chelates **5–7** are nearly isoenergetic. A more definitive distinction would have been more satisfying.

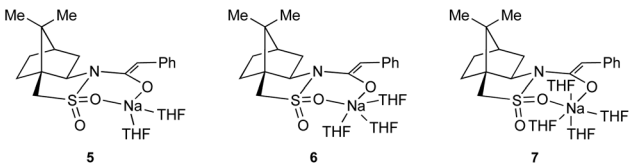

At low THF concentrations or in weaker donor solvents such as MTBE or *N*,*N*-dimethylethylamine (DMEA) resonances of higher aggregates appear. Similarly, binary mixtures of eno-

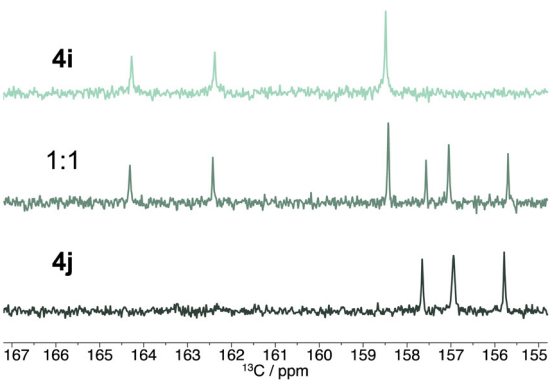

Fig. 1 Partial ^{13}C NMR spectra of 0.20 M of **4i**, a 1 : 1 mixture of enolates **4i** and **4j**, and **4j** in THF at −20 °C. No new peaks appear indicating the absence of heteroaggregation consistent with a monomeric enolate.

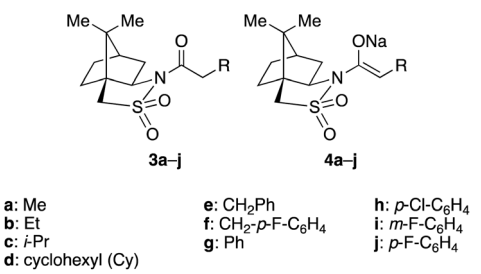

Scheme 1 The *N*-acyl camphorsultam derivatives and their enolates that are studied in this work.

lates in these weak donor ligands afford additional resonances attributed to heteroaggregates. However, the results from lithium Oppolzer enolates revealed extraordinary stereochemical complexity within tetramers examined in excruciating detail.[4] Such potential complexity, lower data quality for the sodium enolates when compared to their lithium counterparts, and occasional solubility problems left us with no appetite for trying to repeat such a study.

THF/HMPA

The predominant protocol for alkylation of sodiated Oppolzer enolates uses THF/HMPA mixtures.[6] MCV analysis using binary enolate mixtures confirm the absence of heteroaggregation. Probing serial solvation by ^{31}P NMR spectroscopy under optimal conditions can provide explicit solvation numbers, but resolution was insufficient to distinguish differential solvation states in this case. DFT computations suggest disolvate **8** and trisolvate **9** to be viable with a 2.5 kcal mol^{-1} preference for **9**. This is not a definitive assignment but provides adequate context for the rate studies. The lithium enolates were shown spectroscopically and computationally to be disolvates analogous to **8**.

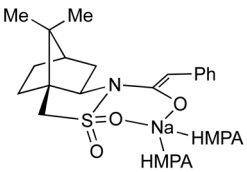

8

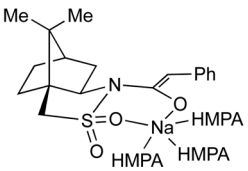

9

TMEDA

N,*N*,*N*′,*N*′-Tetramethylethylenediamine (TMEDA) has a long-standing reputation for promoting deaggregation despite mounting evidence over three decades of a more nuanced story.[13,14] The impetus to examine TMEDA comes from previous studies of both simple and complex sodium enolates which suggest that TMEDA, while not necessarily as strongly binding or as prone toward deaggregating sodium salts, is often superior to THF for controlling structure.[14] Binary mixtures of enolates **4g** and **4i** in TMEDA/toluene show resonance duplications consistent with a heterodimer (Fig. 2). DFT computations show exothermic serial solvation to form doubly chelated dimer. The dimer motif has three possible stereoisomers, **10–12**, owing to chelation with the *endo* or *exo* sulfonyl oxygens (Scheme 2). DFT computations support doubly *exo*-chelated dimer **12** as the preferred form by 10.6 kcal mol^{-1}.

PMDTA

N,*N*,*N*′,*N*″,*N*″-Pentamethyldiethylenetriamine (PMDTA) has a penchant for forming κ^3-solvated monomers,[16] yet binary mixtures of **4g** and **4h** in 3.0 equiv. PMDTA/toluene show marginally resolved but unambiguous heterodimers akin to those observed with TMEDA solvates (ESI†). Computational studies support κ^2,κ^2-solvated dimer **13** akin to TMEDA solvate **12**. (Formally, there could be as many as 10 stereoisomers owing to the lower symmetry of the chelate and the *exo* and *endo* isomerism of the sultam sulfonyl moieties.)

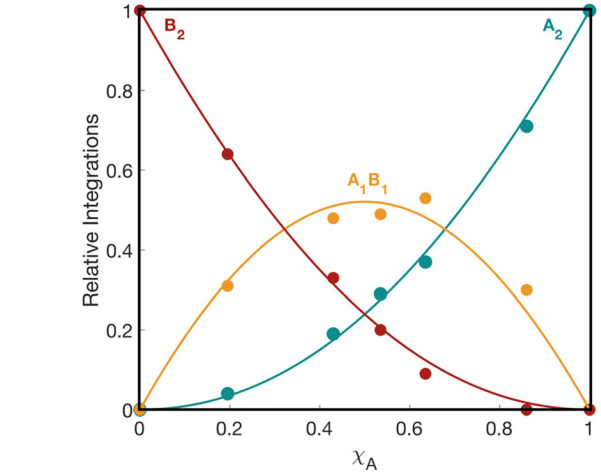

Fig. 2 Job plot showing relative integrations of homodimers of **4g** (A_2, blue) and **4i** (B_2, red) and the heterodimer ($\mathbf{A_1B_1}$, orange) plotted against the measured mole fraction[15] of **4g** (X_A) for 0.20 M mixtures of sodium enolates **4g** and **4i** in 0.88 M TMEDA/toluene at −80 °C monitored by ^{13}C{^{1}H} NMR spectroscopy. The curves result from a parametric fit to a dimer model.

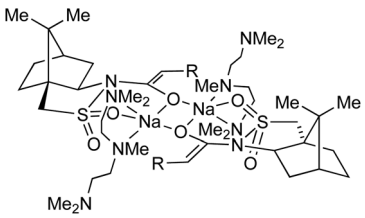

13
(exo,exo-*S*,*S*)

Kinetics of alkylation

The mechanism of alkylation was studied using enolate **4g** and allyl bromide (eqn (3)). The enolate was generated *in situ* using recrystallized NaHMDS.[3a] Rates were monitored by *in situ* IR spectroscopy[17] following the loss of enolate **9** (1616 cm^{-1}) and formation of product **14** (1701 cm^{-1}). A typical decay is illustrated in Fig. 3. Alkylations under non-pseudo-first-order conditions (0.10 M enolate and 3.0 equiv. of allyl bromide) displayed no unusual curvatures emblematic of intervening autocatalysis or autoinhibition.[18]

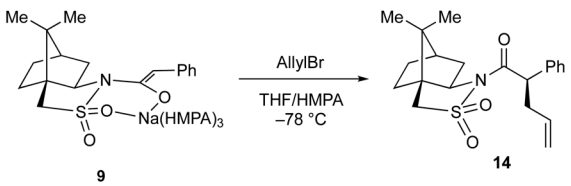

9 **14** (3)

Following protocols developed to study the lithium enolates with enolate **4g** as the limiting reagent, the enolate order, *n*, is determined by best-fit to the non-linear van't Hoff equation (eqn (4)).[19] The curve in Fig. 3 stems from such a fit.

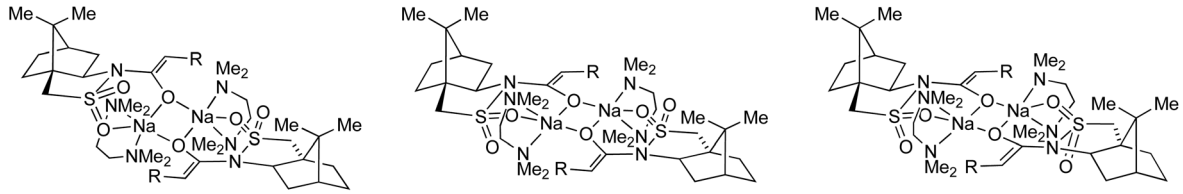

10 (endo,endo-*S*,*S*) **11** (exo,endo-*S*,*S*) **12** (exo,exo-*S*,*S*)

Scheme 2 Stereoisomers of κ^2,κ^2-TMEDA-solvated camphorsultam-enolate dimers. DFT computations support **12** as the preferred form.

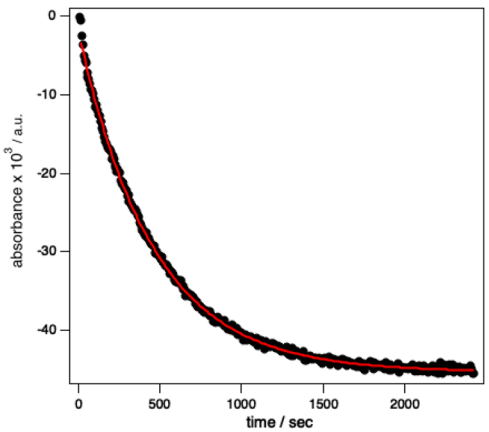

Fig. 3 Alkylation of **4g** (0.025 M; 1616 cm^{-1}) with 0.275 M allyl bromide in 9.24 M THF/toluene at −78 °C to form **14** (1701 cm^{-1}). The red curve depicts an unweighted least-squares fit to eqn (4), such that n = 1.00 ± 0.01, k_{obsd} = 0.0022 ± 0.0009, and $[enolate]_0$ = 0.0430 ± 0.0001.

Considerable variation of n from run to run is compensated by replication, affording n = 1.04 ± 0.25 from the 48 independent decays used to obtain values for k_{obsd}. The first order in excess allyl bromide was confirmed by a three-point control experiment showing a direct relationship of k_{obsd} to concentration. Curiously, comparing the relative rates for the lithium and sodium enolates under otherwise identical conditions afforded $k_{Li/Na}$ = 2.7: the lithium enolate is almost threefold more reactive than the analogous sodium enolate.

$$[\text{enolate}] = \{(n-1)k_{obsd}t + [\text{enolate}]_0^{(1-n)}\}^{1/(1-n)} \qquad (4)$$

As a preface to the rate studies described below it is constructive to consider the backdrop provided by the alkylations of the lithium enolates. In particular, first-order dependencies of the alkylation rates on alkyl halide and enolate monomer implicated a monomer-based alkylation. Second-order dependencies on both THF and HMPA suggested a hexasolvated ion pair. However, the THF dependence proved to be 100% secondary shell (medium) effects rather than primary solvation in which an inverse-first-order-dependence on the toluene cosolvent owing to stabilization of the HMPA in the reactant and a first-order dependence on THF owing to stabilization of the transition structure combined to create an *apparent* second-order THF dependence. Using 2,5-dimethyltetrahydrofuran (2,5-Me_2THF) removed both the influence of toluene and the drifting dielectric constant of the medium,[20] revealing a true zeroth-order dependence on primary-shell solvation by THF. We suspected this primary and secondary-shell solvation narrative would reappear with sodium.

In this event, the first-order dependencies on enolate and allyl bromide followed for the sodium enolates. A second-order HMPA dependence (Fig. 4) implicated a $^+Na(HMPA)_5$ gegenion based on the computed trisolvated monomer **9**. (If disolvate **8** is the dominant form, then we have a $^+Na(HMPA)_4$ gegenion.) The second-order THF dependence in toluene (Fig. 5) and approximate zeroth-order THF dependence using 2,5-Me_2THF with a downward drift (see insert) mirrored the lithium enolates. Once again, the second order in THF is attributed to a first-order medium effect on THF and an inverse-first-order medium effect on toluene (Fig. 6), both of which were negated using 2,5-Me_2THF as cosolvent.

Omitting HMPA

Hoping to eliminate HMPA from the protocol[7] we tried alkylations using TMEDA and PMDTA without much luck. In neat THF the alkylation (eqn (5)) is approximately 100-fold slower than in THF with 10 equiv. of HMPA. However, alkylation with

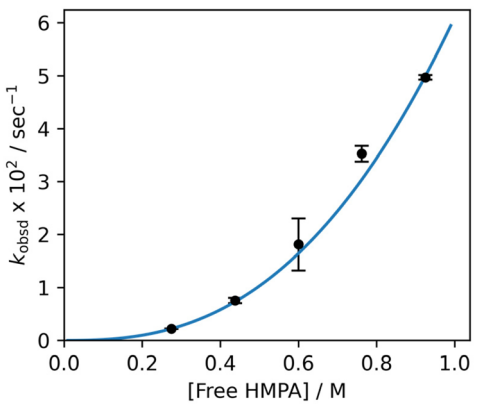

Fig. 4 Plot of k_{obsd} against $[HMPA]_{free}$ for the alkylation of enolate **4g** (0.025 M) with 0.275 M allyl bromide in 9.24 M THF/2,5-Me_2THF at −78 °C.[21] The blue curve depicts an error-weighted least-squares fit to $f(x) = ax^b$ such that a = 0.061 ± 0.001, b = 2.56 ± 0.01.

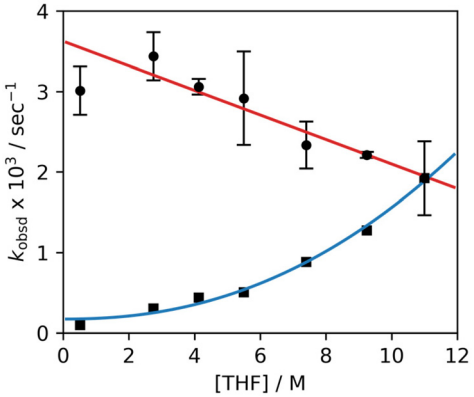

Fig. 5 Plot of k_{obsd} *versus* THF concentration for alkylation of 0.025 M **4g** with allyl bromide (0.275 M) in 0.250 M *free* HMPA[21] at −78 °C in toluene (■) or 2,5-Me_2THF (●) co-solvent. The blue curve depicts an error-weighted least-squares fit to $f(x) = y_0 + ax^b$ such that $y_0 = 1.71 \times 10^{-4} \pm 0.57 \times 10^{-4}$, $a = 8.16 \times 10^{-6} \pm 5.10 \times 10^{-6}$, $b = 2.2 \pm 0.2$. The red curve depicts an error-weighted least-squares fit to $f(x) = y_0 + ax$ such that $y_0 = 3.62 \times 10^{-3} \pm 0.14 \times 10^{-3}$, $a = -1.5 \times 10^{-4} \pm 0.17 \times 10^{-4}$.

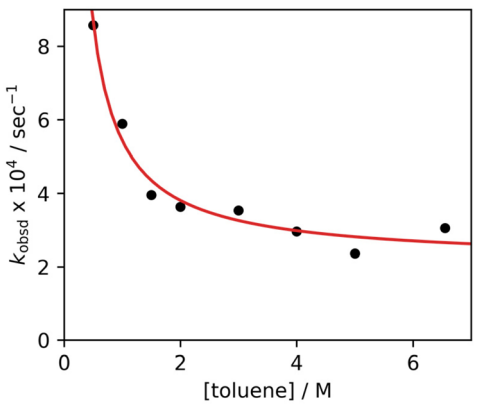

Fig. 6 Plot of k_{obsd} *versus* toluene concentration for the alkylation of 0.025 M **4g** at −78 °C with 0.275 M allyl bromide in 0.250 M *free* HMPA in 0.275 M THF using cyclopentane cosolvent.[21] The curve depicts a least-squares fit to $f(x) = y_0 + ax^b$ such that $y_0 = 2.13 \times 10^{-4} \pm 0.58 \times 10^{-4}$, $a = 3.30 \times 10^{-4} \pm 0.79 \times 10^{-4}$, $b = -0.98 \pm 0.24$.

the highly reactive methyl iodide is sufficiently fast to allow the methylation to occur at −40 °C over 2 hours, which is sufficiently below the −20 °C onset of decomposition.

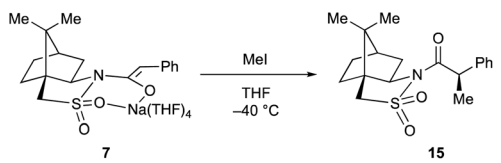

7 15 (5)

The highly abbreviated mechanistic story is that alkylation follows the rate law in eqn (6) (see ESI†), which, given the assignment of enolate **4g** as tetrasolvated monomer, is consistent with a hexa-solvated ion-pair-based mechanism. This is the mechanism found for the HMPA-solvated lithium and sodium enolates with the only difference being the $^+Na(THF)_6$ counterion. Supporting data suggests to us that $^+Na(THF)_6$ is the most probable.[22] As a reminder, the assignment of enolate **4g** in neat THF-solvated monomer as a tetrasolvate was not unassailable, though the $^+Na(THF)_6$ is computationally quite credible.

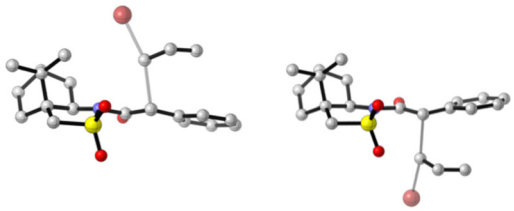

Fig. 7 DFT computed transition structure for the alkylation of enolate **4g** with allylbromide. *Si*-facial approach of the electrophile is favored (2.6 kcal mol^{-1}) over the *Re* face due to stereoelectronic effects emanating from the sultam sulfonyl moiety.[4]

$$-d[enolate]/dt = k'[enolate]^1[THF]^2[MeI]^1 \quad (6)$$

Conclusions

The structural and rate studies of sodiated Oppolzer enolates in THF/HMPA solution are strongly aligned with the results from the lithium enolates in THF/HMPA, differing only in the solvation number of the monomeric reactant and the counterion in the solvent-separated ion-pair.[23] Consequently, the stereochemical model involving an open transition structure crudely depicted as **2** in the introduction and as the ball-and-stick structure in Fig. 7 differs only in the remote ^+MS_n counterion—$^+Li(HMPA)_4$ or $^+Na(HMPA)_5$. The secondary shell influences of toluene on the reactant HMPA and THF on the transition structure are some of the most dramatic we have seen from literally hundreds of rate studies. We will not reiterate the extensive computations pointing to the stereoelectronically preferential attack of the electropile *anti* to the *endo* sulfonyl oxygen.[4] Curiously, several recent reactions that do not involve potentially chelate-forming at all can be explained by the same stereoelectronic control.[24] One might surmise that the only advantage of sodium over lithium is the much higher reactivity but that would be wrong. The lithium and sodium enolates studied show a three-fold greater reactivity of the *lithium* enolate.

We can take some solace in locating a narrow window of reactivity using the highly reactive methyl iodide in which the undesirable HMPA can be excluded as reported by two groups.[7] The greater efficacy of NaPTA when compared with NaHMDS for generating recalcitrant sodium enolates is also notable.

Experimental

Reagents and solvents

NaHMDS and NaPTA were prepared as white crystalline solids.[3a,c] toluene, hexanes, THF, MTBE, and cyclopentane

were distilled from blue or purple solutions containing sodium benzophenone ketyl. Methyl iodide and allyl bromide were distilled from 4 Å molecular sieves. Substrates **3a–j** were prepared according to literature procedures.[1,4]

NMR spectroscopic analysis

An NMR tube fitted with a double-septum under vacuum was flame-dried on a Schlenk line and allowed to cool to room temperature, backfilled with argon, and placed in a dry ice/acetone cooling bath. Individual stock solutions of the *N*-acyl sultams and NaHMDS were prepared at room temperature and 0 °C, respectively. The appropriate amounts of the *N*-acyl sultams, NaHMDS, solvent, and (when applicable) co-solvent were added sequentially *via* a gas-tight syringe. The tube was flame-sealed under a partial vacuum while cold to minimize evaporation. The tubes were mixed on a vortex mixer and stored at −80 °C.

Unless otherwise stated all tubes were sealed with a total enolate concentration of 0.10 M. Standard ^{1}H, ^{19}F, ^{13}C, and ^{31}P direct detection spectra were recorded on a 11.8 T spectrometer at 500.1, 470.6, 125.8, and 202.5 MHz, respectively. ^{1}H, ^{13}C, and ^{31}P resonances are referenced to their respective standards (Me_4Si and H_3PO_4 at 0.0 ppm). ^{19}F spectra are referenced to C_6H_5F (−113.15 ppm).

For quantitated ^{13}C spectra, the spin–lattice relaxation (T1) was determined by standard inversion-recovery experiments on several samples. The relaxation delay (d1) was set to seven times the average relaxation lifetime. Integration of the NMR signals was determined using the line-fitting method included in MNova (Mestrelab research S.L.).

Rate studies

IR spectra were recorded with an *in situ* IR spectrometer (ReactIR iC 10, Mettler Toledo AutoChem) fitted with a 30-bounce, silicon-tipped probe. The spectra were acquired at a gain of 1 and a resolution of 4 cm^{-1}. All tracked reactions were conducted under a positive pressure of argon from a Schlenk line. A representative reaction was carried out as follows:

The IR probe was inserted through a Teflon adapter and O-ring seal into an oven-dried, cylindrical flask fitted with a magnetic stir bar and a T-joint. The T-joint was fitted with a septum for injections and an argon line. After evacuation under full vacuum, heating, and flushing with argon, the flask was charged with the THF/cosolvent mixture of choice (toluene, 2,5-Me_2THF, toluene/cyclopentane) and cooled to −78 °C in a dry ice–acetone bath. A set of 256 baseline scans were collected and IR spectra were recorded every 15 seconds from 30 scans. The reaction vessel was charged to 0.025 M **4g** (1704 cm^{-1}). A 1.00 M stock solution of NaHMDS was injected (0.030 M, 1.2 equiv.) through the septum, and enolization was tracked to completion (1616 cm^{-1}), typically ∼10 min. Following full disappearance of **4g**, HMPA was added to the reaction as a 4.31 M (75 v/v%) stock solution in toluene to avoid freezing. For IR studies of the HMPA-free methylation this step was omitted. The reaction was left to stir for another 10 min. At this point, the spectral collection was halted, and an additional 256 baseline scans were collected. The spectrometer was configured to collect spectra every 5 seconds from 16 scans. 1 set of scans was collected before the addition of *neat* alkylating agent (methyl iodide or allyl bromide) through the septum. The reaction was tracked over 5 half-lives monitoring the disappearance of the enolate (1616 cm^{-1}) and the appearance of the adduct (1701 cm^{-1}).

Density functional theory (DFT) computations

All DFT calculations were carried out using Gaussian 16.[10] Prompted by a recent benchmarking of modern density functionals, all calculations were conducted at the M06-2X level of theory using Grimme's zero-dampened DFT-D3 dispersion corrections.[11a–d] A pruned (99, 590) integration grid (equivalent to Gaussian's "UltraFine" option) was used for all calculations. Where appropriate solvation effects were accounted for by the Self Consistent Reaction Field method using the SMD model of Truhlar and coworkers.[11e] Jensen's polarization-consistent segment-contracted basis set, pcseg-1, was used for geometry optimizations and the expanded pcseg-2 basis set for single-point energy calculations.[11f] Basis set files were obtained from the Basis Set Exchange.[11g] Ball-and-stick models were rendered using CYLview 1.0b.[11h] A large number of DFT-computed energies are archived in the ESI.†[12] A frequency calculation was conducted at all stationary points to ensure the existence of real minima. All reported geometries have exactly zero imaginary (negative) vibrational frequencies.

Author contributions

N. M. Lui: conceptualization (equal), methodology, formal analysis, investigation, visualization, writing – review & editing. D. B. Collum: conceptualization (equal), supervision, funding acquisition, writing – original draft.

Conflicts of interest

The authors declare no competing financial interests.

Acknowledgements

We thank the National Institutes of Health (GM131713) for their support. This work made use of the Cornell University NMR Facility, which is supported, in part, by the National Science Foundation through MRI award CHE-1531632.

References

1 (*a*) W. Oppolzer, Camphor Derivatives as Chiral Auxiliaries in Asymmetric Synthesis, *Tetrahedron*, 1987, **43**, 1969; (*b*) M. M. Heravi and V. Zadsirjan, Recent Advances in the Application of the Oppolzer Camphorsultam as a Chiral Auxiliary, *Tetrahedron: Asymmetry*, 2014, **25**, 1061.

2 Z. Zhang and D. B. Collum, Structures and Reactivities of Sodiated Evans Enolates: Role of Solvation and Mixed Aggregation on the Stereochemistry and Mechanism of Alkylations, *J. Am. Chem. Soc.*, 2019, **141**, 388, and references cited therein.

3 (*a*) R. A. Woltornist and D. B. Collum, Aggregation and Solvation of Sodium Hexamethyldisilazide: Across the Solvent Spectrum, *J. Org. Chem.*, 2021, **86**, 2406; (*b*) R. A. Woltornist, Y. Ma, R. F. Algera, Y. Zhou, Z. Zhang and D. B. Collum, Structure, Reactivity, and Synthetic Applications of Sodium Diisopropylamide, *Synthesis*, 2020, **52**, 1478; (*c*) Y. Ma, N. M. Lui, I. Keresztes, R. A. Woltornist and D. B. Collum, Sodium Isopropyl(trimethylsilyl)amide: A Stable and Highly Soluble Lithium Diisopropylamide Mimic, *J. Org. Chem.*, 2022, **87**, 14223; (*d*) P. Vitale, L. Cicco, F. M. Perna and V. Capriati, Introducing deep eutectic solvents in enolate chemistry: synthesis of 1-arylpropan-2-ones under aerobic conditions, *React. Chem. Eng.*, 2021, **6**, 1796; (*e*) G. Dilauro, C. Luccarelli, A. F. Quivelli, P. Vitale, F. M. Perna and V. Capriati, Introducing Water and Deep Eutectic Solvents in Organosodium Chemistry: Chemoselective Nucleophilic Functionalizations in Air, *Angew. Chem., Int. Ed.*, 2023, **62**, e202304720.

4 N. M. Lui, S. N. MacMillan and D. B. Collum, Lithiated Oppolzer Enolates: Solution Structures, Mechanism of Alkylation, and Origin of Stereoselectivity, *J. Am. Chem. Soc.*, 2022, **144**, 23379.

5 (*a*) A. M. Gouda, E. A. Beshr, F. A. Almalki, H. H. Halawah, B. F. Taj, A. F. Alnafaei, R. S. Alharazi, W. M. Kazi and M. M. AlMatrafi, Arylpropionic Acid-Derived NSAIDs: New Insights on Derivatization, Anticancer Activity and Potential Mechanism of Action, *Bioorg. Chem.*, 2019, **92**, 103224; (*b*) C. Yang, X. Sheng, L. Zhang, J. Yu and H. Huang, Arylacetic Acids in Organic Synthesis, *Asian J. Org. Chem.*, 2020, **9**, 23.

6 For several recent examples of sodium Oppolzer enolate alkylations in total synthesis, see: (*a*) F. Han, G. Liu, C. Jin, J. Wang, J. Liu, L. Wang and Y. Chen, Total Synthesis and Determination of the Absolute Configuration of Rakicidin C, *Org. Lett.*, 2021, **23**, 7069; (*b*) F. Han, G. Liu, X. Zhang, Y. Ding, L. Wang, Y. Wu, Y. Chen and Q. Zhang, Total Synthesis and Structure Revision of Boholamide A, *Org. Lett.*, 2021, **23**, 4976; (*c*) B. Kralt, R. Moreira, M. Palmer and S. D. Taylor, Total Synthesis of A54145 Factor D, *J. Org. Chem.*, 2019, **84**, 12021; (*d*) N. Rival, G. Hanquet, C. Bensoussan, S. Reymond, J. Cossy and F. Coloberta, Diastereoselective Synthesis of the C14–C29 Fragment of Amphidinol 3, *Org. Biomol. Chem.*, 2013, **11**, 6829; (*e*) Y. Ujihara, K. Nakayama, T. Sengoku, M. Takahashi and H. Yoda, First Total Synthesis of Epicoccarine A via *O*- to *C*-Acyl Rearrangement Strategy, *Org. Lett.*, 2012, **14**, 5142.

7 (*a*) K. Pranz and J. Mulzer, Decarboxylative Grob-Type Fragmentations in the Synthesis of Trisubstituted *Z*-Olefins: Application to Peloruside A, Discodermolide, and Epothilone D, *Angew. Chem., Int. Ed.*, 2009, **48**, 5030; (*b*) B. Schmidt and H. Wildemann, Synthesis of Enantiomerically Pure Divinyl- and Diallylcarbinols, *J. Chem. Soc., Perkin Trans. 1*, 2002, 1050.

8 O. Tai, R. Hopson and P. G. Williard, Ligand Binding Constants to Lithium Hexamethyldisilazide Determined by Diffusion-Ordered NMR Spectroscopy, *J. Org. Chem.*, 2017, **82**, 6223.

9 J. S. Renny, L. L. Tomasevich, E. H. Tallmadge and D. B. Collum, Method of Continuous Variations: Applications of Job Plots to the Study of Molecular Associations in Organometallic Chemistry, *Angew. Chem., Int. Ed.*, 2013, **52**, 11998.

10 M. J. Frisch, G. W. Trucks, H. B. Schlegel, G. E. Scuseria, M. A. Robb, J. R. Cheeseman, G. Scalmani, V. Barone, G. A. Petersson, H. Nakatsuji, X. Li, M. Caricato, A. V. Marenich, J. Bloino, B. G. Janesko, R. Gomperts, B. Mennucci, H. P. Hratchian, J. V. Ortiz, A. F. Izmaylov, J. L. Sonnenberg, D. Williams-Young, F. Ding, F. Lipparini, F. Egidi, J. Goings, B. Peng, A. Petrone, T. Henderson, D. Ranasinghe, V. G. Zakrzewski, J. Gao, N. Rega, G. Zheng, W. Liang, M. Hada, M. Ehara, K. Toyota, R. Fukuda, J. Hasegawa, M. Ishida, T. Nakajima, Y. Honda, O. Kitao, H. Nakai, T. Vreven, K. Throssell, J. A. Montgomery Jr., J. E. Peralta, F. Ogliaro, M. J. Bearpark, J. J. Heyd, E. N. Brothers, K. N. Kudin, V. N. Staroverov, T. A. Keith, R. Kobayashi, J. Normand, K. Raghavachari, A. P. Rendell, J. C. Burant, S. S. Iyengar, J. Tomasi, M. Cossi, J. M. Millam, M. Klene, C. Adamo, R. Cammi, J. W. Ochterski, R. L. Martin, K. Morokuma, O. Farkas, J. B. Foresman and D. J. Fox, *Gaussian 16, Revision C.01*, Gaussian, Inc., Wallingford CT, 2016.

11 (*a*) N. Mardirossian and M. Head-Gordon, Thirty Years of Density Functional Theory in Computational Chemistry: An Overview and Extensive Assessment of 200 Density Functionals, *Mol. Phys.*, 2017, **115**, 2315; (*b*) Y. Wang, P. Verma, X. Jin, D. G. Truhlar and X. He, Revised M06 Density Functional for Main-Group and Transition-Metal Chemistry, *Proc. Natl. Acad. Sci. U. S. A.*, 2018, **115**, 10257; (*c*) Y. Zhao and D. G. Truhlar, The M06 Suite of Density Functionals for Main Group Thermochemistry, Thermochemical Kinetics, Noncovalent Interactions, Excited States, and Transition Elements: Two New Functionals and Systematic Testing of Four M06-Class Functionals and 12 Other Function, Truhlar, *Theor. Chem. Acc.*, 2008, **120**, 215; (*d*) S. Grimme, J. Antony, S. Ehrlich and H. A. Krieg, A Consistent and Accurate Ab Initio Parametrization of Density Functional Dispersion Correction (DFT-D) for the 94 Elements H-Pu, *J. Chem. Phys.*, 2010, **132**, 154104; (*e*) A. V. Marenich, C. J. Cramer and D. G. Truhlar, Universal Solvation Model Based on Solute Electron Density and a Continuum Model of the Solvent Defined by the Bulk Dielectric Constant and Atomic Surface Tensions, *J. Phys. Chem. B*, 2009, **113**, 6378; (*f*) F. Jensen, Unifying General and Segmented Contracted Basis Sets. Segmented Polarization Consistent Basis Sets, *J. Chem. Theory Comput.*, 2014, **10**, 1074; (*g*) B. P. Pritchard, D. Altarawy, B. Didier, T. D. Gibson and T. L. Windus, New

Basis Set Exchange: An Open, Up-to-Date Resource for the Molecular Sciences Community, *J. Chem. Inf. Model.*, 2019, **59**, 4814; (*h*) C. Y. Legault, *CYLview, 1.0b*, Université de Sherbrooke, Québec (Canada), 2009.

12 For references to computations of sodium enolate alkylations, see. (*a*) G. Sini, A. Tessier, J. Pytkowicz and T. Brigaud, Fluorine···and π···Alkali Metal Interactions Control in the Stereoselective Amide Enolate Alkylation with Fluorinated Oxazolidines (Fox) as a Chiral Auxiliary: An Experimental and Theoretical Study, *Chem. – Eur. J.*, 2008, **14**, 3363; (*b*) A. Burmudžija, S. Marković, J. Muškinja, A. Pejović and J. Tošović, Influence of counterion on the methylation of some ambident nucleophiles: DFT study, *React. Kinet., Mech. Catal.*, 2018, **123**, 201; (*c*) Y. Zhou, I. Keresztes, S. N. MacMillan and D. B. Collum, Disodium Salts of Pseudoephedrine-Derived Myers Enolates: Stereoselectivity and Mechanism of Alkylation, *J. Am. Chem. Soc.*, 2019, **141**, 16865; (*d*) Also, ref. 2 and 9.

13 D. B. Collum, Is *N*,*N*,*N*′,*N*′-Tetramethylethylenediamine a Good Ligand for Lithium?, *Acc. Chem. Res.*, 1992, **25**, 448.

14 (*a*) L. L. Tomasevich and D. B. Collum, Method of Continuous Variation: Characterization of Alkali Metal Enolates Using ^{1}H and ^{19}F NMR Spectroscopies, *J. Am. Chem. Soc.*, 2014, **136**, 9710; (*b*) See also ref. 2, 3*a*, and 18*c*.

15 The intended mole fraction refers to the mole fraction based on what was added to the samples. The measured mole fraction — the mole fraction within only the ensemble of interest — eliminates the distorting effects of impurities.

16 (*a*) Y. Ma, R. A. Woltornist, R. F. Algera and D. B. Collum, Reactions of Sodium Diisopropylamide: Liquid-Phase and Solid–Liquid Phase-Transfer Catalysis by *N*,*N*,*N*′,*N*″,*N*″-Pentamethyldiethylenetriamine, *J. Am. Chem. Soc.*, 2021, **143**, 13370; (*b*) P. C. Andrews, M. Koutsaplis and E. G. Robertson, Thermodynamically Favored Anion Rearrangements in Li and Na Complexes of (S)-N-α-(Methylbenzyl)allylamine, *Organometallics*, 2009, **28**, 1697; (*c*) P. C. Andrews, C. L. Raston, B. A. Roberts, B. W. Skelton and A. H. White, Heavier alkali metal complexes of the bulky alkyl ligand 2-(bis(trimethylsilyl) methyl)-6-methylpyridine: Crystal structures of [{6-Me(2 Pyr)}$(Me_3Si)_2$CNa(pmdta)] and [{6-Me(2-Pyr)}$(Me_3Si)_2$CK]$_\infty$, *J. Organomet. Chem.*, 2006, **691**, 3325.

17 A. J. Rein, S. M. Donahue and M. A. Pavlosky, In Situ FTIR Reaction Analysis of Pharmaceutical-Related Chemistry and Processes, *Curr. Opin. Drug Discovery Dev.*, 2000, **3**, 734.

18 Several general-purpose reviews on determining reaction mechanism: (*a*) S. J. Meek, C. L. Pitman and A. J. M. Miller, Deducing Reaction Mechanism: A Guide for Students, Researchers, and Instructors, *J. Chem. Educ.*, 2016, **93**, 275; (*b*) E. M. Simmons and J. F. Hartwig, On the Interpretation of Deuterium Kinetic Isotope Effects in C–H Bond Functionalizations by Transition Metal Complexes, *Angew. Chem., Int. Ed.*, 2012, **51**, 3066; (*c*) D. B. Collum, A. J. McNeil and A. Ramírez, Lithium Diisopropylamide: Solution Kinetics and Implications for Organic Synthesis, *Angew. Chem., Int. Ed.*, 2007, **46**, 3002; (*d*) R. F. Algera, L. Gupta, A. C. Hoepker, J. Liang, Y. Ma, K. J. Singh and D. B. Collum, Lithium Diisopropylamide: Non-Equilibrium Kinetics and Lessons Learned about Rate Limitation, *J. Org. Chem.*, 2017, **82**, 4513.

19 (*a*) J. H. van't Hoff, E. Cohen and T. Ewan, *Studies in Chemical Dynamics*, Frederik Muller & Co., Amsterdam, NL, 1896; (*b*) S. K. Upadhyay, *Chemical Kinetics and Reaction Dynamics*, Springer Netherlands, Dordrecht, NL, 2007.

20 The dielectric constants of substituted tetrahydrofurans are slightly lower than THF. (*a*) Y. Harada, M. Salomon and S. Petrucci, Molecular Dynamics and Ionic Associations of Lithium Hexafluoroarsenate ($LiAsF_6$) in 4-Butyrolactone Mixtures with 2-Methyltetrahydrofuran, *J. Phys. Chem.*, 1985, **89**, 2006; (*b*) C. Carvajal, K. J. Tolle, J. Smid and M. Szwarc, Studies of Solvation Phenomena of Ions and Ion Pairs in Dimethoxyethane and Tetrahydrofuran, *J. Am. Chem. Soc.*, 1965, **87**, 5548.

21 The ligand concentrations in the plots refer to *free* donor solvent concentration. "[enolate]" refers to the concentration of the monomer subunit (normality).

22 There are an enormous number of documented $^{+}$Na(THF)$_6$. For an example, see: Z. Livingstone, A. Hernan-Gomez, S. E. Baillie, D. R. Armstrong, L. M. Carrella, W. Clegg, R. W. Harrington, A. R. Kennedy, E. Rentschler and E. Hevia, Assessing the Reactivity of Sodium Alkyl-Magnesiates Towards Quinoxaline: Single Electron Transfer (SET) vs. Nucleophilic Alkylation Processes, *Dalton Trans.*, 2016, **45**, 6175.

23 Nevertheless, this did not have to be the case. For examples of divergence between organolithium and organosodium reactivity see. (*a*) R. A. Woltornist and D. B. Collum, Ketone Enolization with Sodium Hexamethyldisilazide: Solvent- and Substrate-Dependent *E*–*Z* Selectivity and Affiliated Mechanisms, *J. Am. Chem. Soc.*, 2021, **143**, 17452; (*b*) N. Davison, C. L. McMullin, L. Zhang, S. X. Hu, P. G. Waddell, C. Wills, C. Dixon and E. Lu, Li vs Na: Divergent Reaction Patterns between Organolithium and Organosodium Complexes and Ligand-Catalyzed Ketone/Aldehyde Methylenation, *J. Am. Chem. Soc.*, 2023, **145**, 6562 and (*c*) ref. 3*a* and *b*.

24 (*a*) M. Sampath, S. R. Jayaraman, V. R. Eda, R. Potham, R. R. Budhdev, S. Sen, R. Bandichhor and S. Oruganti, Enantioselective Synthesis of the Chiral Pyrrolidine Fragment of Upadacitinib via Chiral Auxiliary Directed Diastereoselective 1,3-Dipolar Cycloaddition, *Org. Process Res. Dev.*, 2022, **26**, 1794; (*b*) M. Oga, Y. Takamatsu, A. Ogura and K.-I. Takao, Asymmetric Synthesis of Cyclopentene Compounds Containing All-Carbon Quaternary Stereocenters by (3+2) Cycloaddition and Its Application in the Formal Synthesis of (*R*)-(-)-Puraquinonic Acid, *J. Org. Chem.*, 2022, **87**, 8788.

